Deliverable 1.3: DAS synthetic dataset

DigiMon

Digital monitoring of CO_2 storage projects

Prepared by Alan F. Baird[a], Rob Mellors[b], Bob Paap[c], Vincent Vandeweijer[c], Arie Verdel[c], Antony Butcher[a], and Anna L. Stork[d]

[a]University of Bristol
[b]Lawrence Livermore National Laboratory
[c]TNO
[d]Silixa Ltd.

DigiMon Deliverable D.1.3 Version 1.2,

August 2020

Revision

Version	Date	Change	Page
1.0	03.2020	First version	All
1.1	04.2020	Added revised SW4 North Sea model and expanded conclusions and recommendations	
1.2	08.2020	Changed format to DigiMon report template	All

Document distribution

ACT Coordinator

- Research Council of Norway

ACT national funding agencies

- Forschungszentrum Jülich GmbH, Projektträger Jülich, (FZJ/PtJ), Germany.
- Geniki Grammatia Erevnas kai Technologias/The General Secretariat for Research and Technology (GSRT), Greece.
- Ministry of Economic Affairs and Climate/Rijksdienst voor Ondernemend Nederland (RVO), the Netherlands.
- The Research Council of Norway (RCN), Norway.
- Gassnova, Norway.
- Development and Executive Agency for Higher Education, Research, Development and Innovation Funding (UEFISCDI), Romania.
- Department for Business, Energy and Industrial Strategy (BEIS), UK.
- Department of Energy (DoE), USA.

DigiMon partners

- NORCE Norwegian Research Centre AS
- OCTIO Environmental Monitoring AS
- NTNU Norwegian University of Science and Technology
- University of Bristol
- CRES Centre for Renewable Energy Sources and Saving
- Helmholtz–Centre for Environmental Research
- Sedona Development SRL
- TNO Nederlandse Organisatie voor toegepast -natuurwetenschappelijk Onderzoek
- Geotomographie GmbH
- LLC Lawrence Livermore National Security
- SILIXA LTD
- EQUINOR ASA
- REPSOL –NORGE AS

Table of contents

List of tables

1 Introduction

Deliverable D1.3 of the ACT DigiMon project is a synthetic microseismic distributed acoustic sensins (DAS) dataset. There are a number of possible uses for such a dataset; for example supporting the development and testing of DAS processing algorithms, testing the efficacy of different array geometries in detecting and characterising events, or simulating a field experiment to better understand observed processes. Given the large number of possible uses it was decided that rather than simply delivering a collection of files of synthetic seismic events, it would be more valuable to deliver a modelling framework from which synthetic data can be generated as the need arises, combined with a small example dataset of a few events to demonstrate the capabilities.

DAS systems record seismic wavefields and ground motion due to their sensitivity to strain along the axis of the fibre. To understand the response of DAS it is necessary to understand (1) the seismic source, (2) the path effects and (3) the site and instrument effects. In this report we discuss the modelling of the first two contributions of the DAS response; the source and path effects. We simulate the resulting particle motion and strain at the fibre location, resulting from realistic microseismic sources in geological models representative of the North Sea. The third contribution; site and instrument effects, is contained in the transfer function, which describes the mathematical relationship between the wavefield properties at the cable location to the recorded DAS output. The form of the transfer function is a key unanswered question which will be addressed in Task 1.2 of the DigiMon project.

2 Geological model

For the generic geologic model representative of the North Sea we use VELMOD-3 (Pluymaekers et al, 2017), which describes a layer cake P-velocity model of the Dutch North Sea, based on a compilation of velocity data from a wide range of geologic units. The P wave velocity of most of the geological units is described by a simple linear function:

$V(Z)=V_0+k\,Z$

Where V is the velocity at depth Z, V_0 is the “normalized velocity”, and k is the velocity depth gradient. V_0 and k are determined empirically by linear regression of velocity-depth data.

This parameterisation makes it easy to generate simple 1D P-wave velocity models for an arbitrary selection of stratigraphic layers. However, the model does not include S-wave velocities. To estimate these, we adopt empirical relationships between P and S velocities for sedimentary rocks given by Castagna et al. (1985). Figure 1 shows an example 1D model generated following this methodology.

Note that for future site-specific models, the velocity model would be better derived using sonic-velocity and density logs from local borehole data.

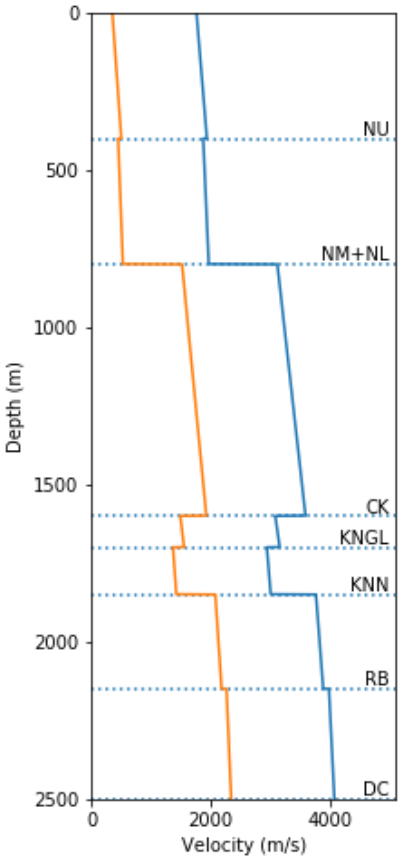

Figure 1 - A representative North Sea velocity model, based on VELMOD-3. Vp (blue line) and Vs (orange line).

3 Modelling software

There are a number of choices of software for simulating seismic wave propagation. We choose two popular open source software packages to test: SW4 and SPECFEM3D Cartesian. SW4 (Sjögreen & Petersson, 2012; Petersson & Sjögreen, 2018) uses a node based finite difference approach to solve the seismic wave equations to fourth-order accuracy. SPECFEM3D (Komatitsch & Tromp 1999; Tromp et al. 2008; Peter et al. 2011) uses the spectral element method. Additionally, for simple models analytical and semianalytical modelling approaches are possible (e.g. ray-theory and wavenumber integration methods), which can be used for benchmarking.

4 Modelling approach

A three-stage approach is adopted to assess the suitability of the modelling programs and refine the selection of model parameters. Initially, a simple homogeneous model is used to compare the synthetics produced by the different software packages. This allows for identification of the causes of inconsistencies between the models, and once remedied we gradually increase the complexity of the model.

The three stages proposed in this modelling approach are:

1. Homogeneous medium; using a moment tensor source. This can also be compared with analytical methods (e.g. ray theory).
2. Three-Layer model with force source. Layers are homogeneous (no velocity gradient). This will allow comparisons involving reflections/transmissions at interfaces, as well as surface waves.
3. North Sea model; after consistent results have been generated from the two previous stages and the velocity model has been finalised.

5 Results

5.1 Homogeneous model

For initial testing a homogeneous velocity model was used with the following specifications:

- Homogeneous velocity model Vp=1966.76 m/s, Vs=646.45 m/s, density=1960 kg/m3
- Absorbing boundary conditions for all boundaries (Note SW4 used free surface boundary condition for the top boundary)
- Vertical array channels located (metres): n=0, e=0, d=0,10,20,...,990
- Source parameters:
    - Location: n=150, e=-200, d=700
    - Focal mechanism: Strike/Dip/Rake = 295˚/60˚/-105˚
    - Scalar moment: 1e12 Nm (Mw=2)
    - Gaussian displacement wavelet with central frequency of 7 Hz

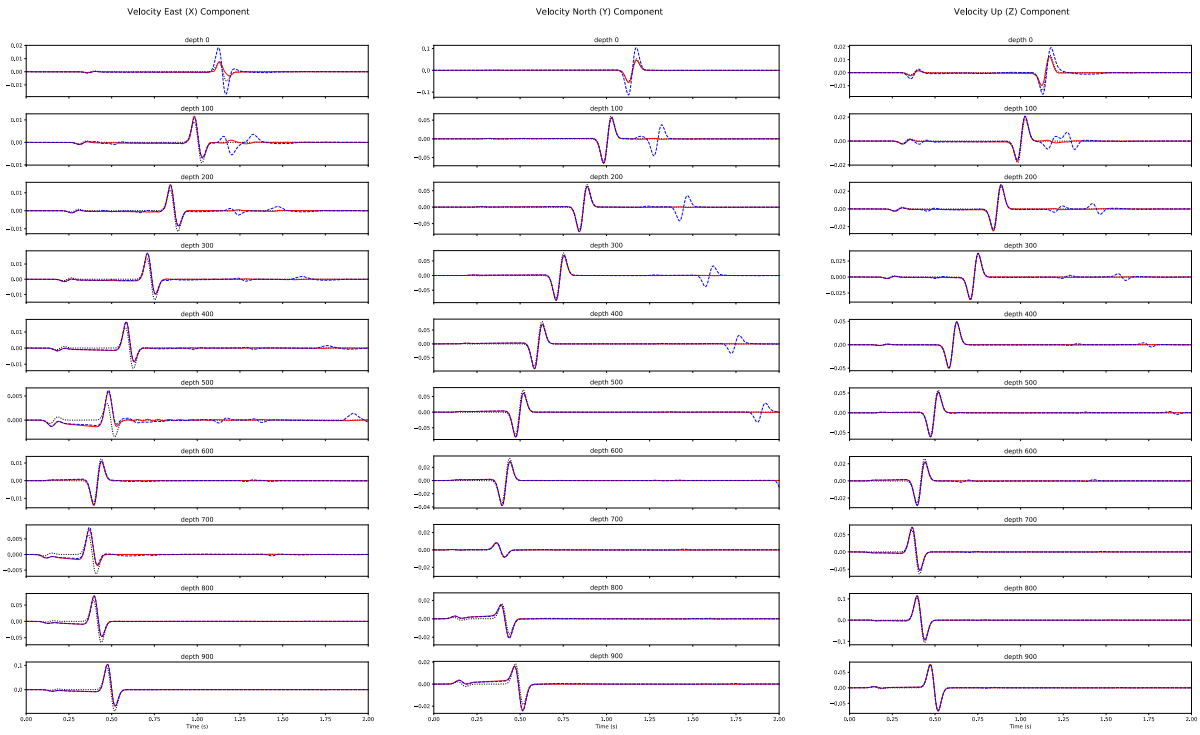

Figure 2 - Comparison of synthetic particle-velocity waveforms for the homogeneous model computed using SPECFEM3d (red solid line), SW4 (blue dashed line) and Ray-theory synthetics (dotted black line).

For this homogeneous simulation, synthetics were also produced using ray-theory to provide an analytical solution to compare with. Figure 2 shows a comparison of the particle velocity synthetics for every 10th receiver in the vertical array (100 m spacing). The three models produce very consistent results except for a few key differences. There is an inconsistency in the amplitudes in the SW4 synthetics at the shallowest receiver (depth=0m), which is due to the SW4 model using a free surface boundary condition at the top interface instead of the prescribed absorbing boundary condition. This introduces amplitude differences at the surface as well as a reflected wave propagating downwards, which is not seen in the SPECFEM3D and ray-synthetics. Additionally, the ray synthetics show a small difference in amplitude between the P and S arrivals at receivers close to source depth (most clearly seen on the X component of receivers 500 and 700 m depth of Figure 2). This is because ray theory synthetics use a far-field approximation to the solution of the wave equation (i.e. there are additional effects near the source that are not accounted for). However, the difference is relatively small, and both SW4 and SPECFEM produce consistent results at this depth, which gives us confidence that they are correctly modelling the near field effect.

5.2 Three Layer Model

Next, a simple three layer model was constructed using SPECFEM3D and SW4 using the following specifications, with model geometry shown in Figure 3:

- Velocity model
  - 1st (top) layer
    - Depth range: 0m -> 20m
    - Vp = 750 m/s, Vs = 441 m/s, density = 2200 kg/m3
  - 2nd layer
    - Depth range: 20m -> 200m
    - Vp = 2000 m/s, Vs = 1176 m/s, density = 2200 kg/m3
  - 3rd (bottom) layer
    - Depth range: 200m -> at least 400m (absorbing boundary)
    - Vp = 4000 m/s, Vs = 2353 m/s, density = 2200 kg/m3
- Boundary conditions
  - Free surface at top
  - Some form of absorbing boundary condition at base and sides
    - Stacey boundaries for SPECFEM
    - Supergrid boundaries for SW4
- Receivers
  - Surface linear array coordinates (m)
    - N= 0.; E = 0, 1, 2,…, 999, 1000; D = 0 m
  - Vertical array
    - N=0; E= 800; D = 0, 1, 2,…, 399, 400 (4 m spacing for SW4)
- Source parameters
  - Surface source (buried 1 m)
    - vertical unit force (1 N) pointing down N=0, E = 1000, D=0
    - 7 Hz gaussian (same as previous model)
  - Buried source
    - same as surface force but located: N=0, E = 1000, D = 350

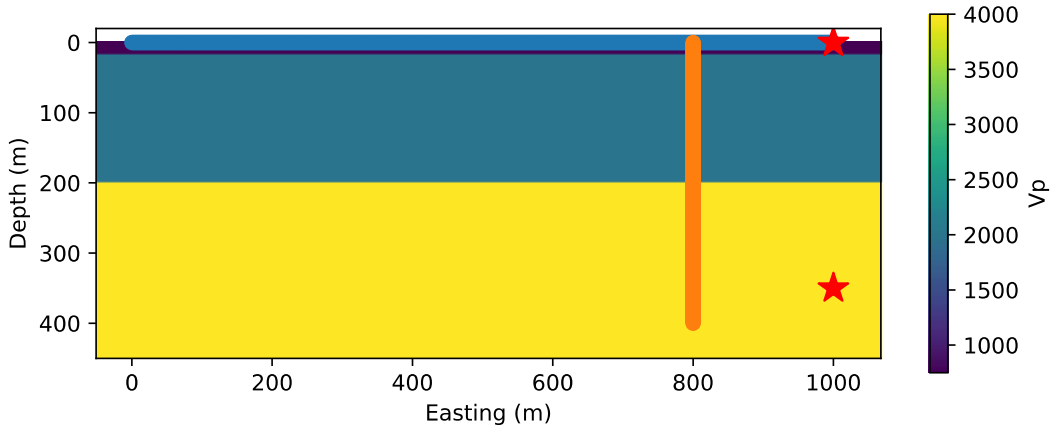

Figure 3 - Cross sectional view of three layer model, showing P velocities (background colour), source locations (red stars) and array geometry (surface array in blue and vertical array in orange).

For this model, the mesh was generated in SPECFEM using an element size of 25 m. This element size is based on guidelines of required element sizes for spectral element models to accurately simulate the smallest estimated wavelengths expected, here corresponding to the S wave velocity in the shallowest and slowest layer. The SW4 model was generated with a grid spacing of 4 m throughout most of the model, but with mesh refinement in the upper layer to achieve a grid spacing of 1 m. This was required to allow a station spacing of 1 m along the surface array, but also has the effect of increasing the accuracy for waves propagating in the shallow layers.

Figure 4 shows the *in-line* component (i.e. E component for surface array and Z component for borehole array) of velocity synthetics for the surface source. They generally show quite good agreement for the body wave arrivals, however the surface waves show a poorer fit. There is some evidence of grid dispersion in the SPECFEM model. This is most apparent in the surface waves present along the surface array, which show a clear phase lag in the SPECFEM synthetics compared to SW4. Additionally, there are reverberations present in the SPECFEM synthetics which continue after the main waves have passed and are not seen in SW4. This suggests that a smaller element size may be needed in SPECFEM to accurately model surface waves and S waves in the slower layers.

Figure 5 shows a similar trace comparison of the velocity synthetics for the buried source. They show generally match reasonably well except for some variation towards the western end of the surface array where SPECFEM shows more complex waveforms, suggesting there may be some boundary effects. The vertical array traces match well, except for some evidence of grid dispersion in the SPECFEM model in the shallower channels.

Figure 6Figure 9 show comparison plots of velocity and strain-rate synthetics for each source and array combination. For the SPECFEM model, strain-rate synthetics were calculated by computing the spatial gradient of the in-line component of the velocity synthetics using 2nd order accurate central differences with 1m channel spacing. SW4 outputs strain seismograms directly, and we converted these to strain-rate by applying an additional time derivative. Overall the synthetics using both methods seem to agree reasonably well. However, there are some clear boundary condition issues with the SPECFEM model. This is most apparent in the surface array recording of the buried source (Figure 8), where there is a clear boundary reflection at the western end of the model (located at channel 0), as well as at the eastern end (located 200 m east of channel 2000).

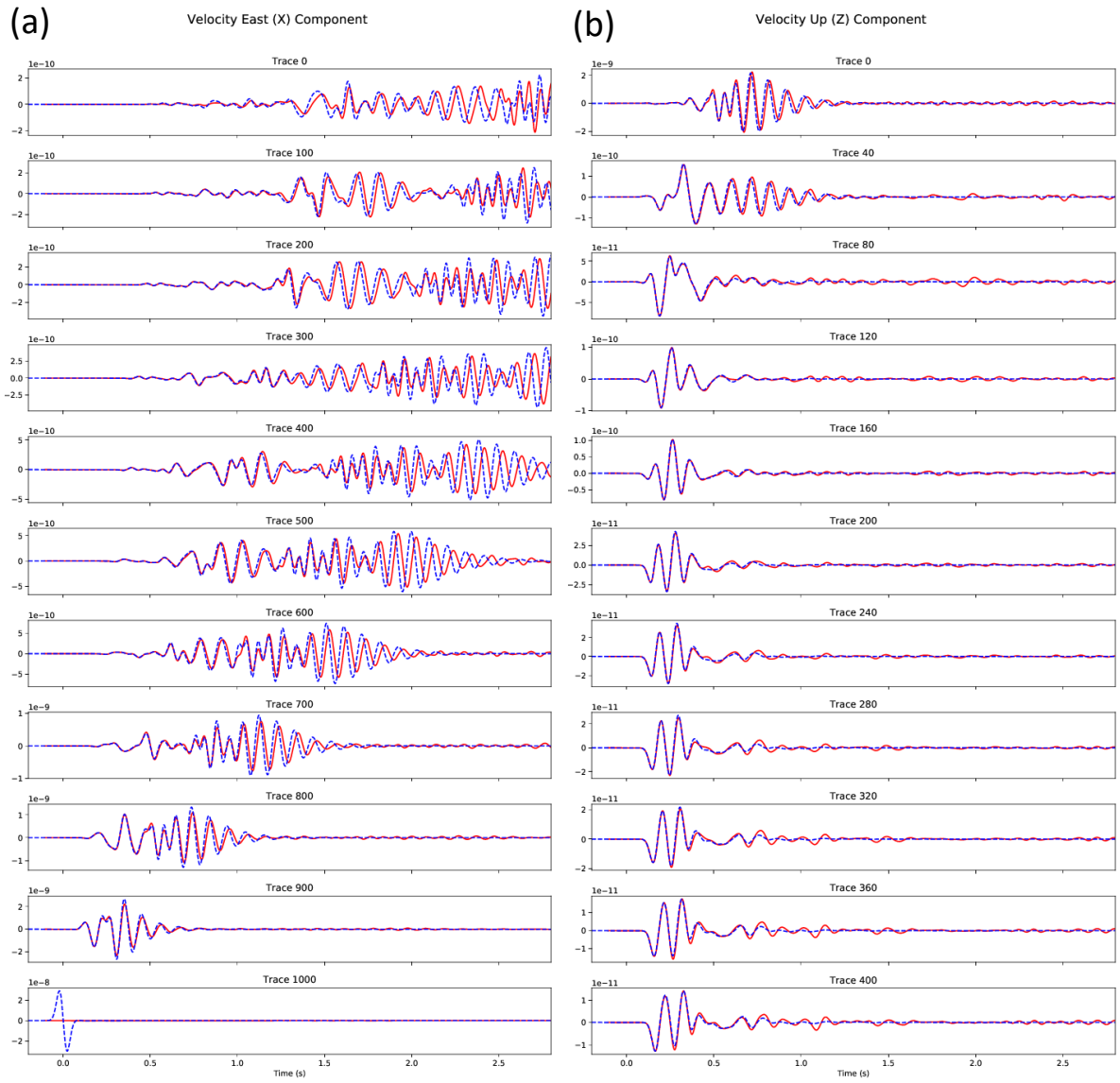

Figure 4 – Trace overlay comparisons of in-line velocity synthetics for the three-layer model with surface source along the (a) surface array (E component) and (b) borehole array (Z component). Red lines indicate SPECFEM3D and blue dashed lines indicate SW4. Note the source was located at trace 1000 of the surface array.

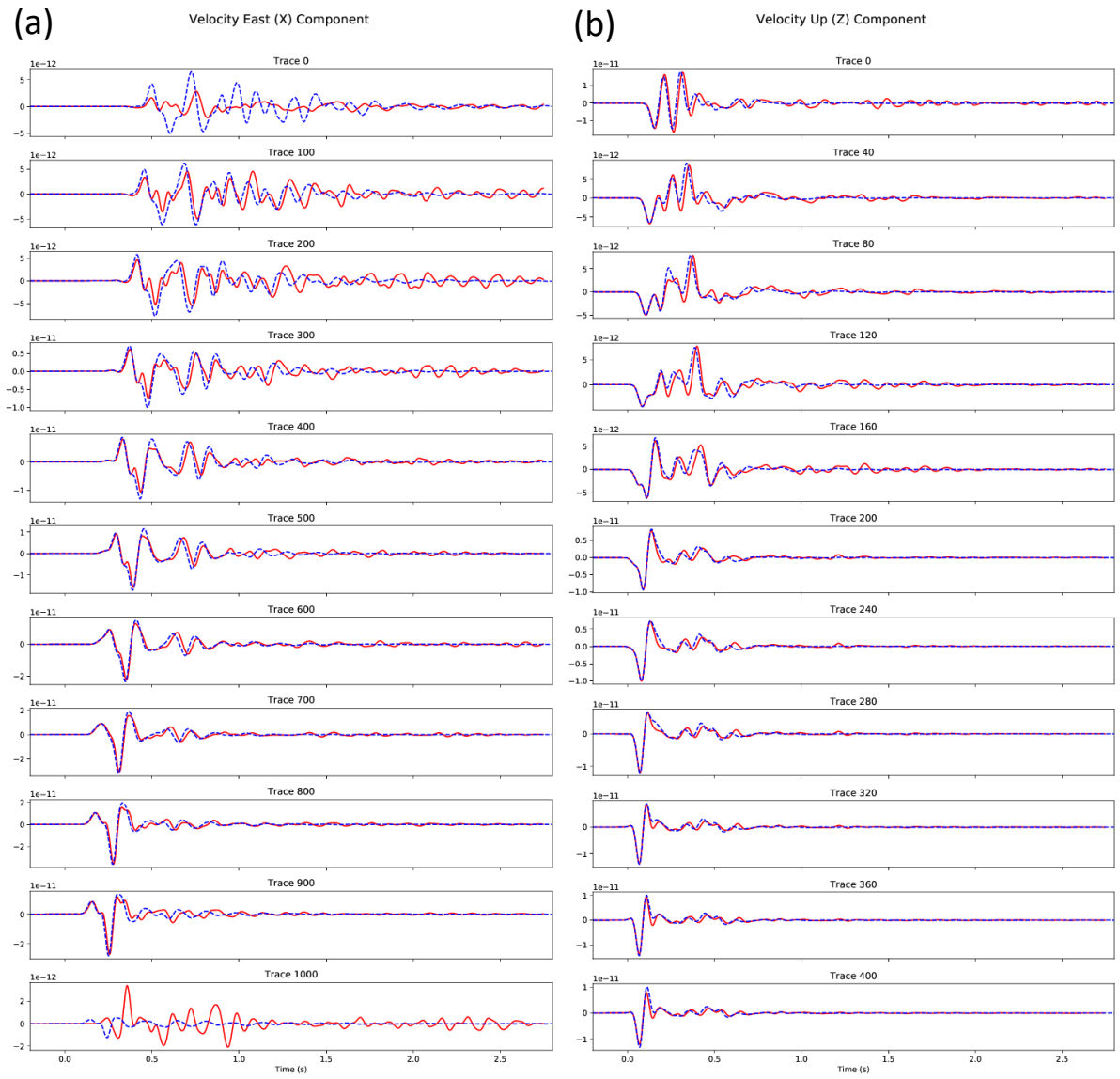

Figure 5 – Trace overlay comparisons of in-line velocity synthetics for the three-layer model with buried source along the (a) surface array (E component) and (b) borehole array (Z component). Red lines indicate SPECFEM3D and blue dashed lines indicate SW4. Note the source was located at trace 1000 of the surface array.

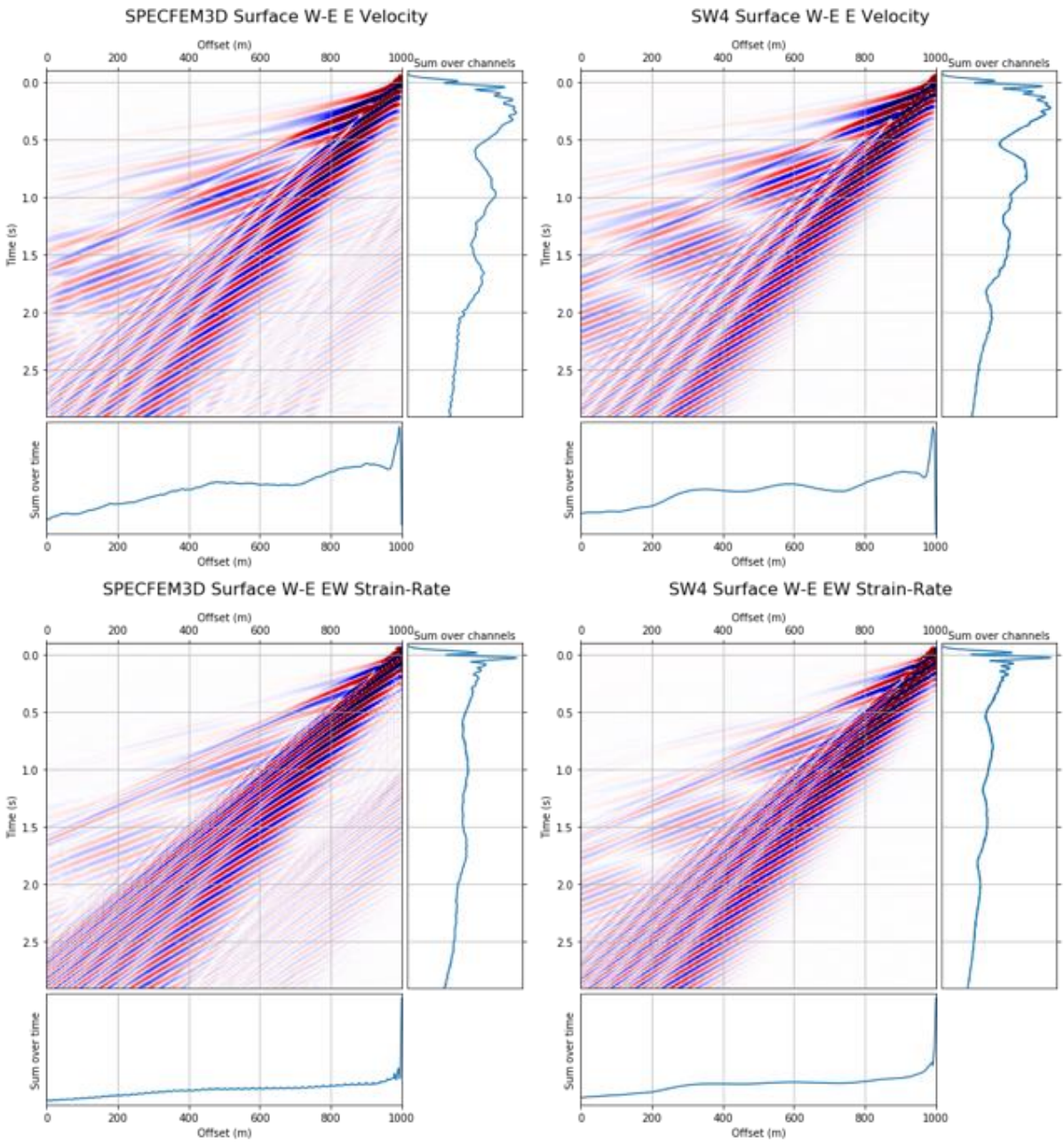

Figure 6 – Comparisons of synthetics produced by Specfem (left) and SW4 (right) showing in-line velocity (top) and axial strain (bottom) for the three-layer model with surface source recorded along the surface array. Channel 0 is located at the east end of the array, with the source located at channel 1000.

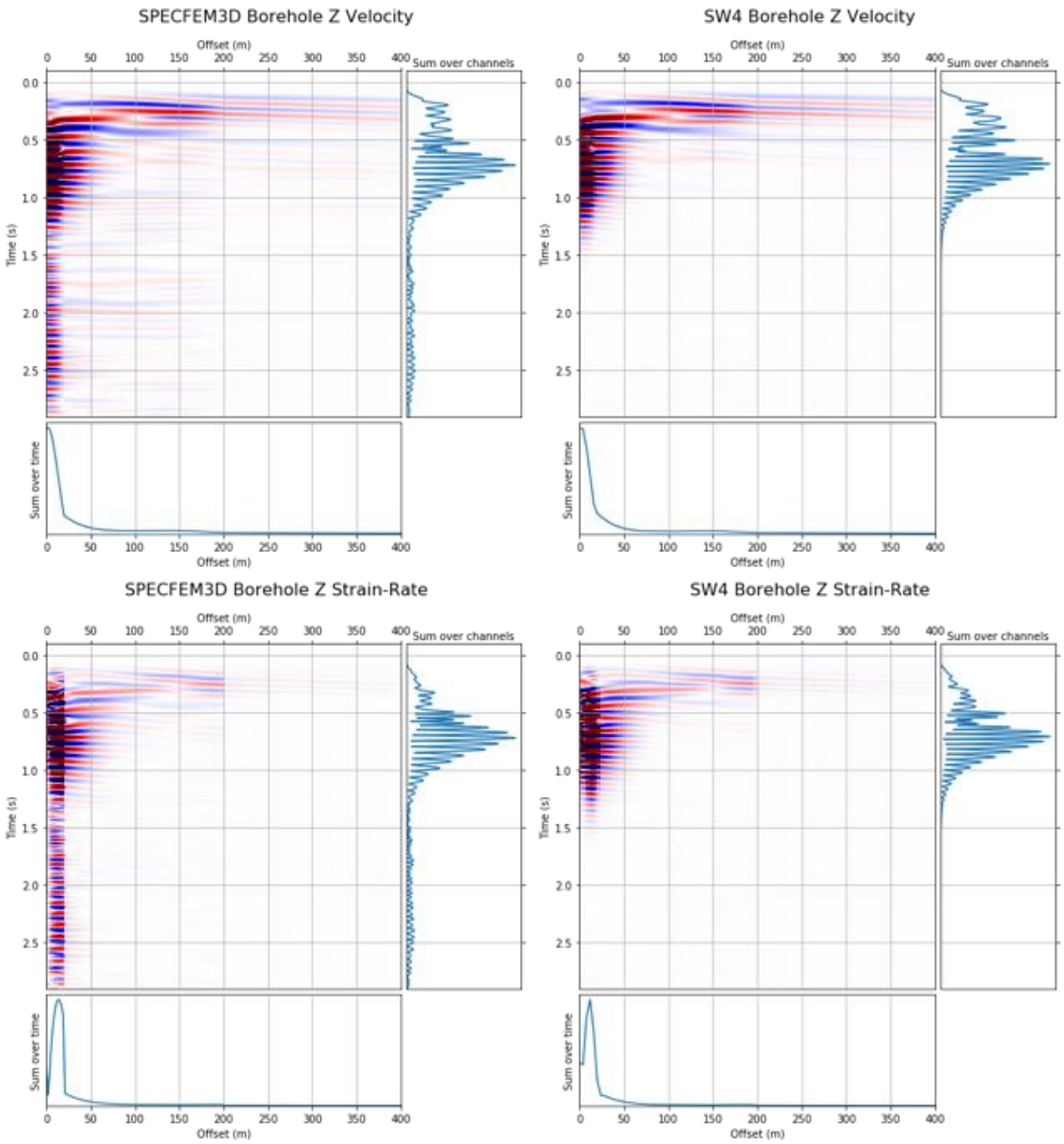

Figure 7 – Comparisons of synthetics produced by Specfem (left) and SW4 (right) showing in-line velocity (top) and axial strain (bottom) for the three-layer model with surface source recorded along the borehole array. Channel 0 is located at the surface, with the base of the array at 400 m depth. The source is located at 200 m east of the top of the array.

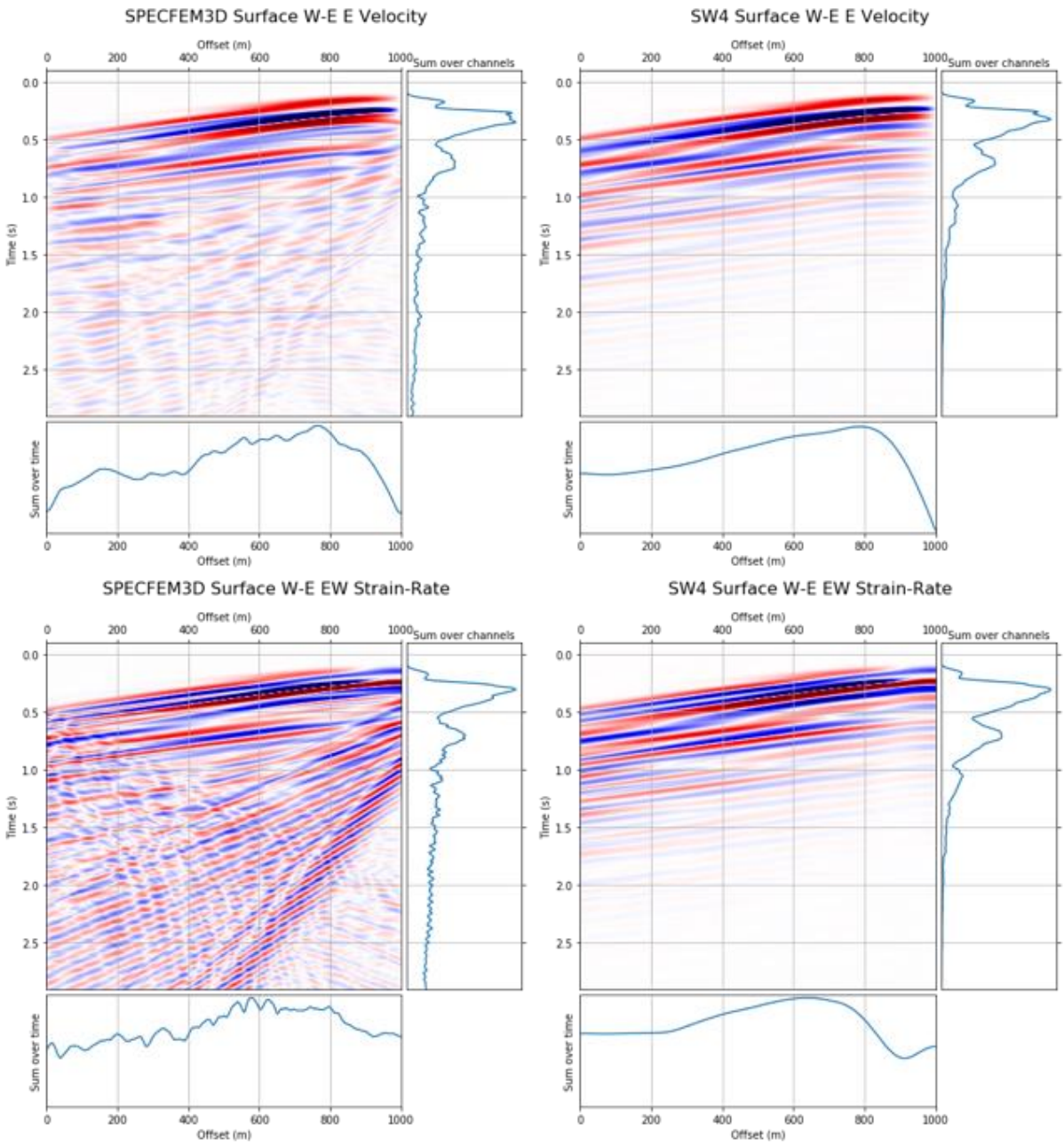

Figure 8 – Comparisons of synthetics produced by Specfem (left) and SW4 (right) showing in-line velocity (top) and axial strain (bottom) for the three-layer model with buried source recorded along the surface array. Channel 0 is located at the east end of the array, with the source located 350 m below channel 1000.

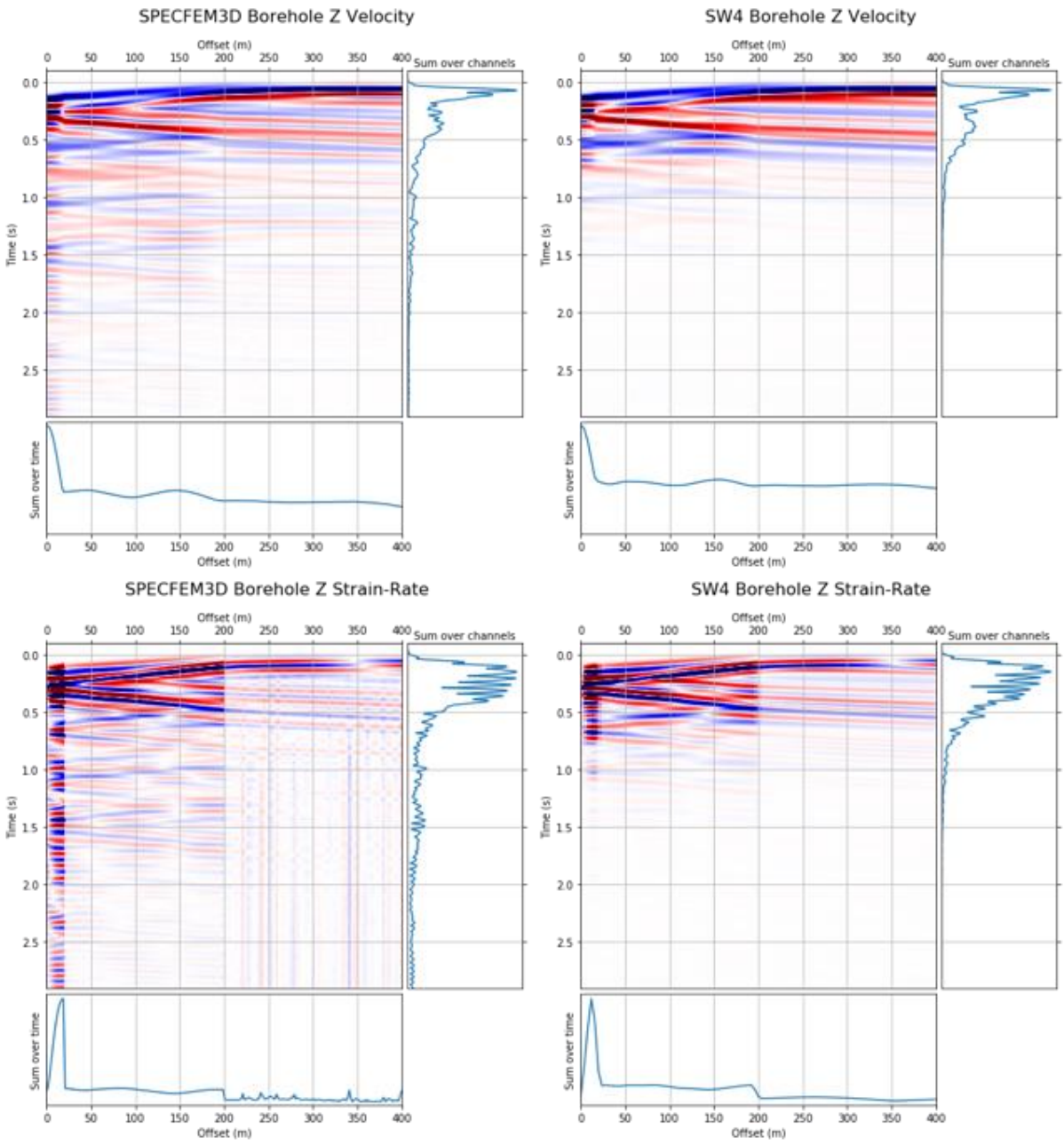

Figure 9 – Comparisons of synthetics produced by Specfem (left) and SW4 (right) showing in-line velocity (top) and axial strain (bottom) for the three-layer model with buried source recorded along the borehole array. Channel 0 is located at the surface, with the base of the array at 400 m depth. The source is located at 200 m east of channel 350.

5.3 North Sea Model

Finally a generic "North Sea" model was constructed using the following specifications, with model geometry shown in Figure 10Figure 11:

- Velocity model
    - As shown in figure 1. Based on VELMOD-3 which provides layer cake P-velocities for Dutch North Sea
    - S-velocities estimated from empirical relationship between P and S velocities (Costagna relations)
    - Density is arbitrarily chosen (first 2 layers 1960 kg/m^3, lower layers 2600 kg/m^3)
- Receivers (origin at top of vertical array)
    - Vertical array
        - Channel coordinates E=0, N=0, D=0,1,2,…,1999,2000 (1 m spacing)
    - Two surface linear arrays running N-S and E-W, centred over vertical array
        - Coordinates = -1152m to +1152 at 1m spacing
- Source parameters
    - Location: E=-136, N=170, D=1630
    - Focal mechanism: Strike/Dip/Rake = 110˚/73˚/20˚
    - Scalar moment: 1e12 Nm (Mw=2)
    - Gaussian displacement wavelet with central frequency of 7 Hz

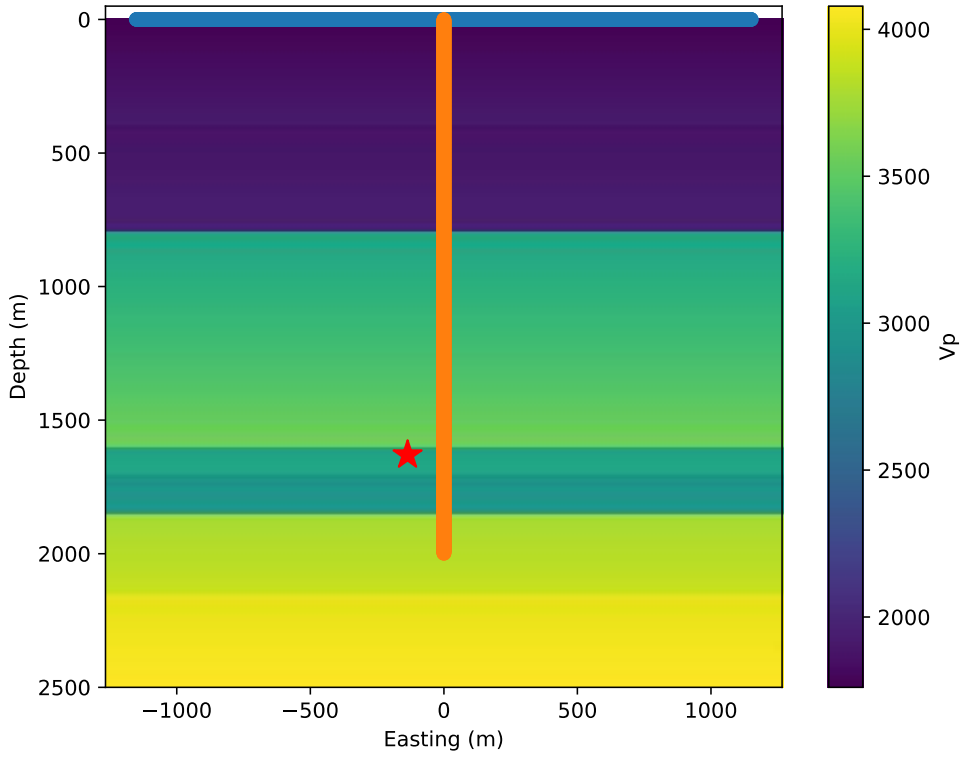

Figure 10 – East-West cross section through the North Sea model showing P velocities (background colour), source location (red star) and array geometry (E-W array in blue and borehole array in orange).

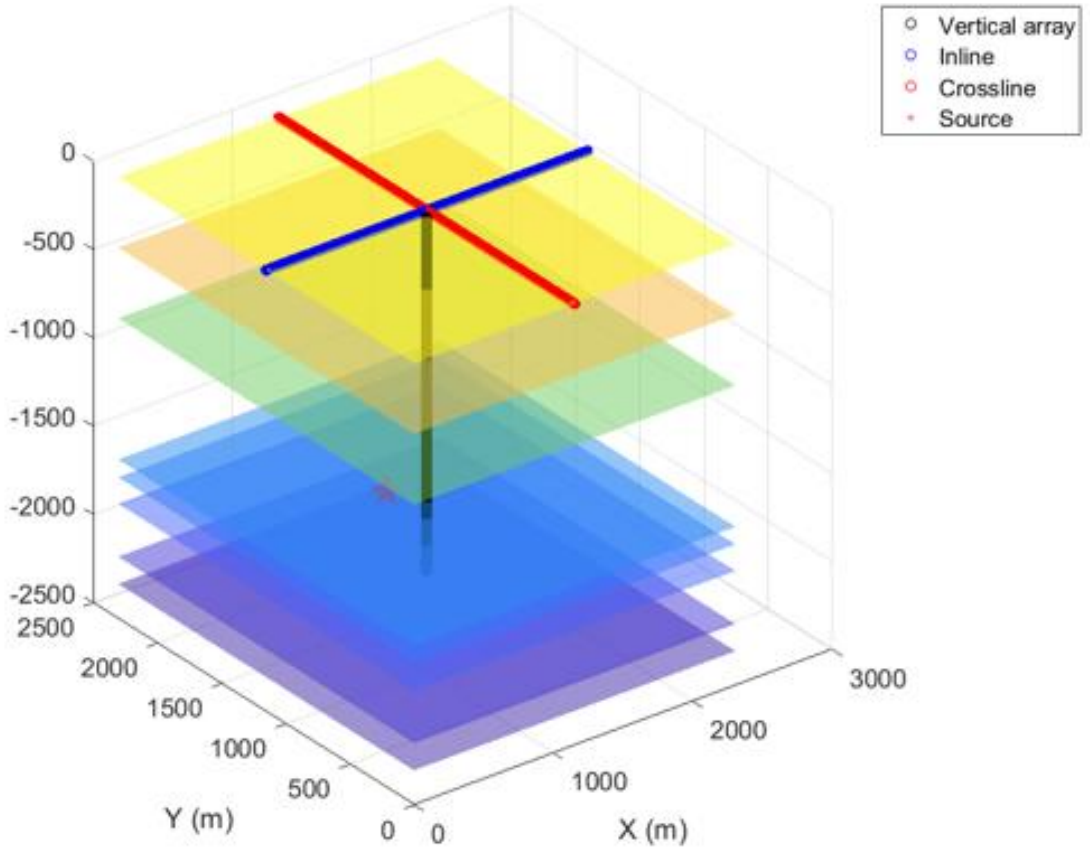

Figure 11 – 3D view of the model showing array geometry, and major lithological interfaces of the velocity model.

At the time of preparing this report, a full size SPECFEM model has been run, with the full array geometry in place using an element size of 25 m. In addition, a SW4 test model including just the vertical array with a smaller later extent has been run, using a variable grid spacing with depth, of 8m at the base decreasing to 4m at 1850m depth and 2m above 1600m. ***Please note that following the preparation of this report, a revised SW4 model was run which resolves some discrepancies shown in this section. The revised SW4 models have been added to the report in Section 0.***

Figure 12 shows a trace comparison of the vertical velocity synthetics along the borehole array. The travel-times between the two models seem to agree, and the amplitudes are the same order of magnitude, however the details of the amplitudes and shape of the waveforms do not match. This is still an unresolved issue that is being investigated but may be due to insufficient grid resolution within the deeper low velocity layers (between 1600m and 1850m), where the source is located. At this stage it is unclear whether the issue is with SPECFEM or SW4 (or both).

Figure 13 show comparison plots of velocity and strain-rate synthetics for the vertical array, with the method of generating strain-rate the same as in the three-layer model. Due to the unresolved issue the

two models do not match in detail; though they are broadly similar. There appears to be some numerical artefacts present in the SPECFEM model, particularly in the low velocity zones (both near-surface and 1600-1850m). This is most evident in the strain-rate synthetics and is likely due to a combination of boundary reflections and grid dispersion.

For the two surface arrays, we currently only have synthetics produced from the SPECFEM model which are shown in Figure 14. Much like the three-layer model there are clear boundary reflections visible, due to the Stacey boundary conditions applied at each end of the arrays. For both surface arrays the central channel coincides with the first channel in the borehole array shown in Figure 13. As clearly shown in the borehole array the first arrival is the direct P wave at ~0.7 s, followed by a S-to-P converted wave from the 800m interface arriving at ~0.9 s. However, these arrivals are barely observable in the surface array, due to the low broadside P wave sensitivity issue inherent to DAS systems with straight fibres. In contrast, the S arrivals, first the P-S converted phase at ~2.0 s followed by the much stronger direct S arrival at ~2.25 s, can both be clearly observed.

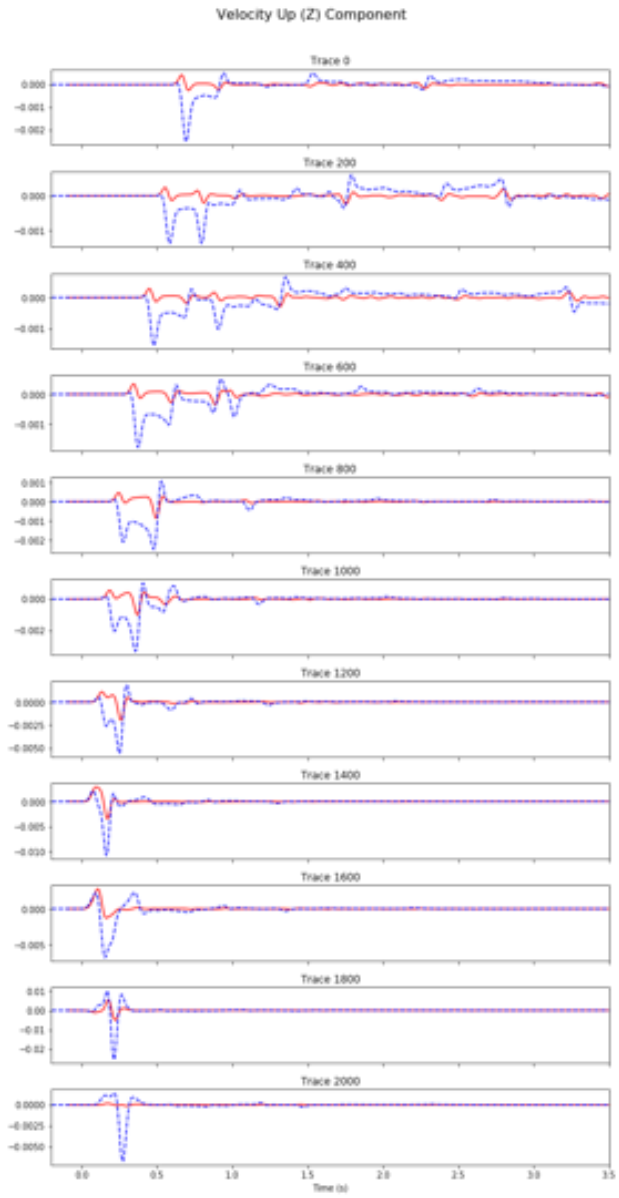

Figure 12 – Trace overlay comparisons of in-line velocity synthetics for the North Sea model along the borehole array (Z component). Red lines indicate SPECFEM3D and blue dashed lines indicate SW4. Note the source was located at a depth of 1630m. Note that a revised SW4 model discussed in Section 0 resolves much of the discrepancy between SPECFEM3D and SW4 (see Figure 16).

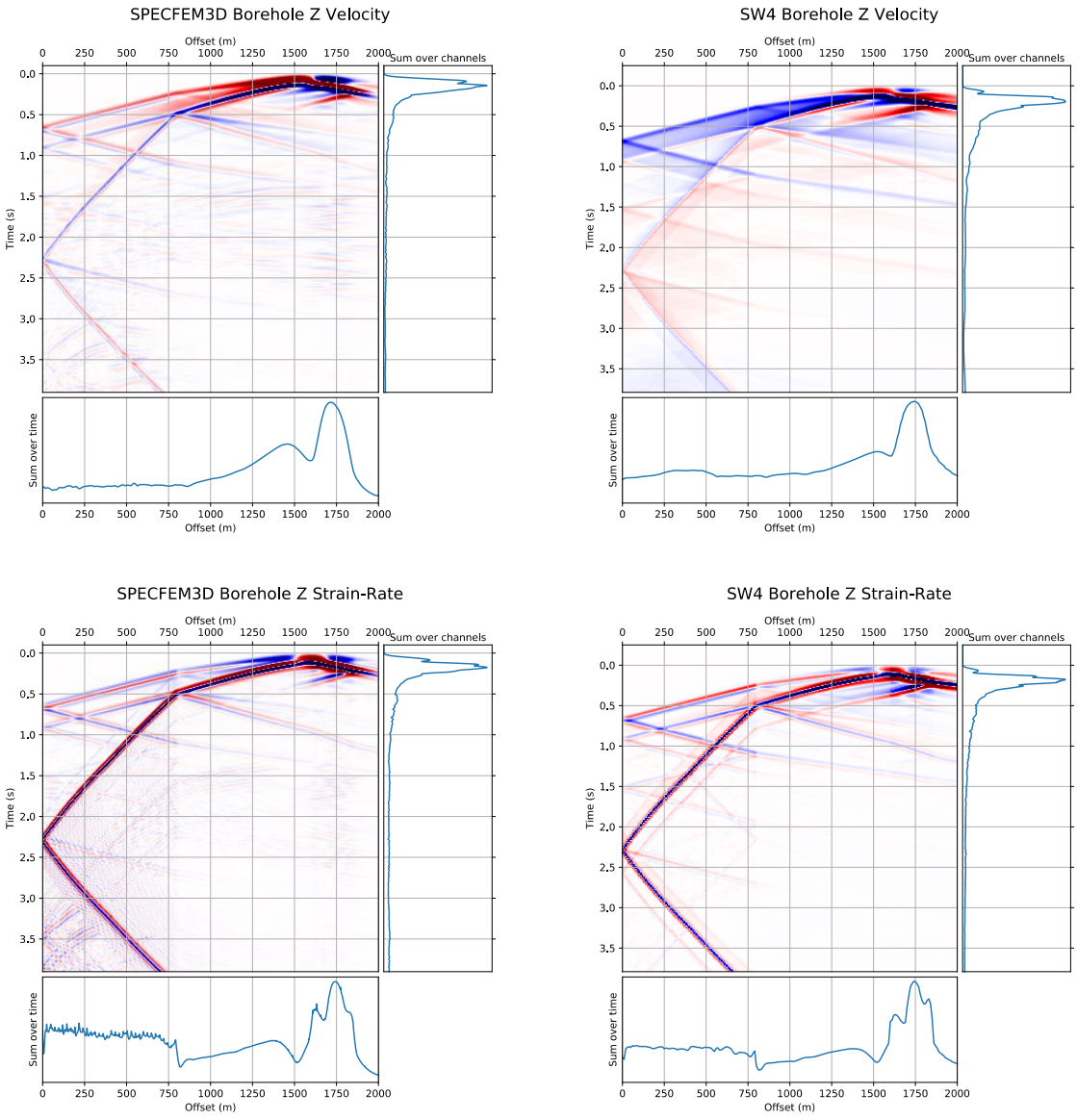

Figure 13 – Comparisons of synthetics produced by Specfem (left) and SW4 (right) showing in-line velocity (top) and axial strain (bottom) for the North Sea model recorded along the borehole array. Channel 0 is located at the surface, with the base of the array at 2000 m depth. The source is located at a depth of 1630 m. Note that a revised SW4 model discussed in Section 0 resolves much of the discrepancy between SPECFEM3D and SW4 (see Figure 17).

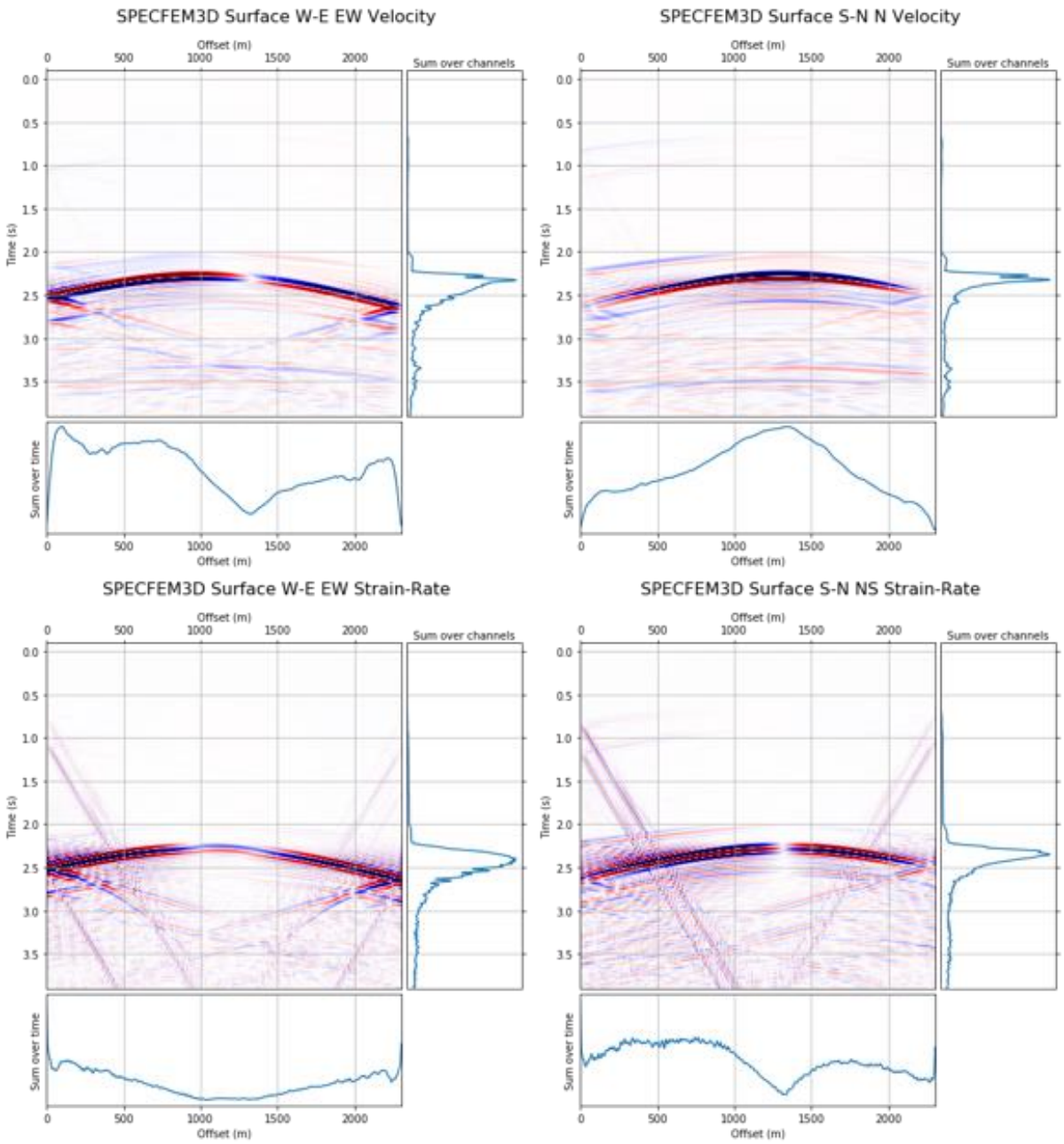

Figure 14 - Specfem synthetics along the W-E array (left) and S-N array (right) showing in-line velocity (top) and axial strain (bottom) for the North Sea model. The central channel (channel 1152) coincides with the top of the borehole array.

6 Addendum March 2020: Revised SW4 North Sea model

One of the possible reasons for the mismatch between SW4 and SPECFEM3D was that there was insufficient grid resolution within the deeper low velocity layers where the source is located. SW4 supports variable mesh size but in a constrained manner. The lowest grid size is set and defined as the lowermost grid. Mesh refinement steps are set which reduce the grid size by half. In this way, for example, a grid size of 8 can be reduced to a surface grid of 2 by two refinement settings. Although this decreases the time need for calculations, two difficulties exist:

1) SW4 receivers must be at mesh nodes. A grid spacing of 8 means that the receivers cannot be closer than 8 meters.
2) The refinement generally assumes that velocities increase with depth and that the points per wavelength does not vary significantly with each layer. The North Sea model has a pronounced low velocity zone which makes a smooth variation of points per wavelength impossible. This may lead to some error.

Figure 15 compares seismograms at the surface for three possible mesh refinement scenarios:

1) Grid spacing of h = 2 m with no grid refinement
2) Grid spacing of h = 4 m at the base, refined to h = 2 m above z=800 m
3) Grid spacing of h = 8 m at the base, refined to h = 4 m and 2 m at 1800 m and 800 m depth, respectively

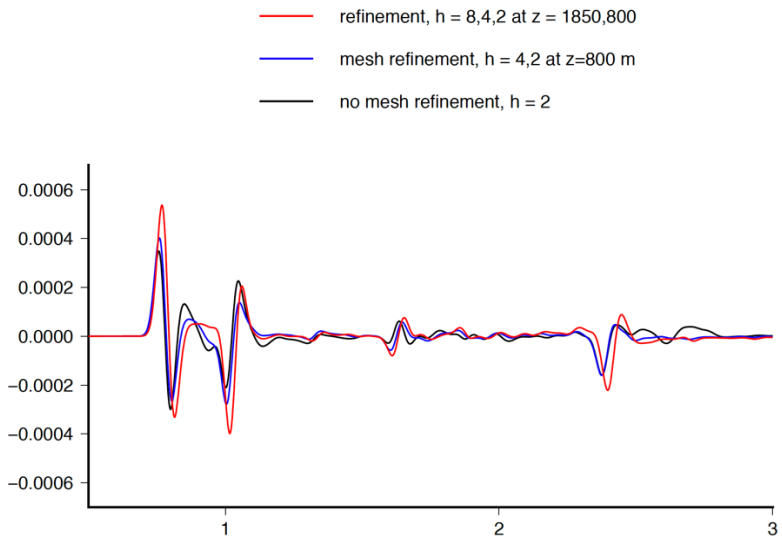

Figure 15 - Comparison of seismogram at the surface for three different mesh refinement scenarios.

I/O constraints may significantly increase the time of computation. Similar models but with different number of receivers differ significantly in required time. One workaround for this is to define different grid specifications for borehole versus surface arrays. A borehole model requires a small grid size at depth to allow for closely spaced receivers. In this case, the horizontal extent may be restricted to ensure a relatively small model. If surface receivers over a wide extent are needed, then mesh refinement can be used, as the uppermost layer is always the smallest grid size.

Figure 16 shows a trace comparison of the three component velocity synthetics along the borehole array between the SPECFEM3D model and a revised SW4 model with a grid spacing of h=2 m with no grid refinement. The horizontal extent of the model was constrained to allow small model size, thus surface receivers were not modelled. We see a greatly improved match between the two models in this scenario. Note, however, that there is some evidence of grid dispersion present in the SPECFEM3D model at shallower (and low velocity) depths. Figure 17 shows the strain-rate synthetics along the full depth of the borehole.

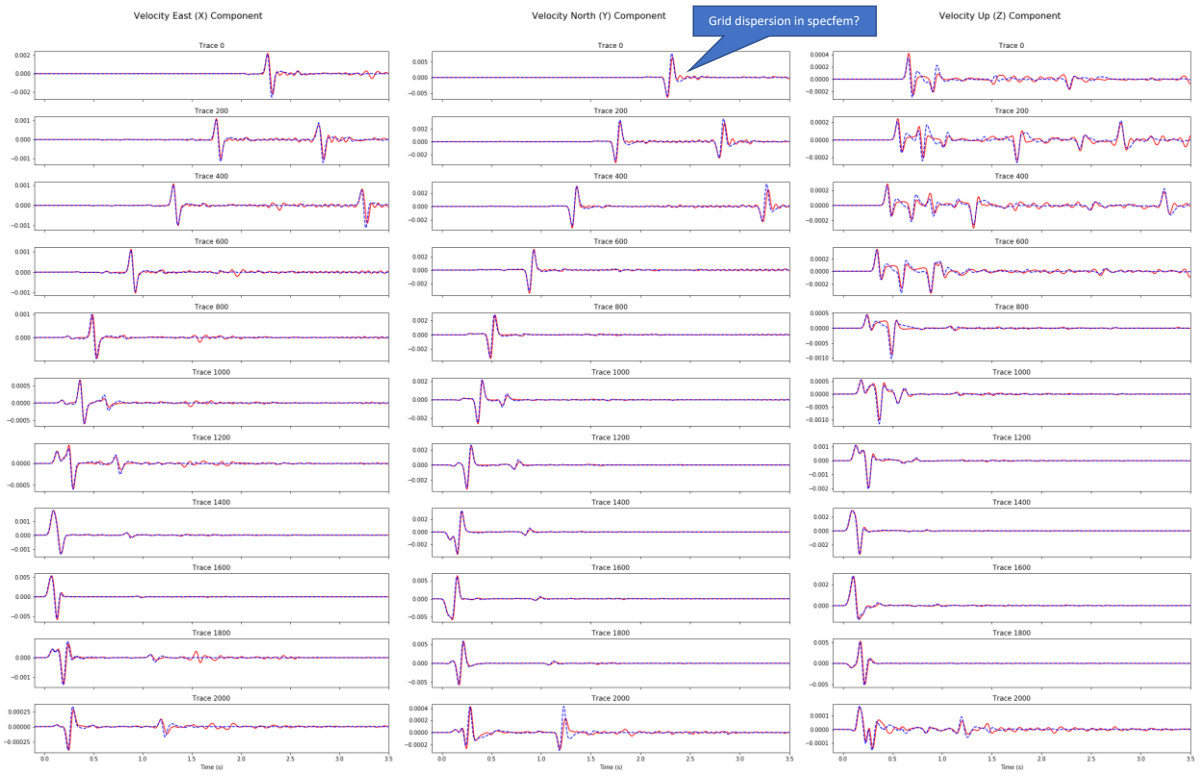

Figure 16 - Trace overlay comparisons of 3C velocity synthetics for the North Sea model along the borehole array (E,N and Z components). Red lines indicate SPECFEM3D and blue dashed lines indicate the revised SW4 model with h=2m and no grid refinement. The source was located at a depth of 1630m. There is quite good agreement between the models, however, there appears to be evidence of grid dispersion in the SPECFEM3D model in the shallow receivers.

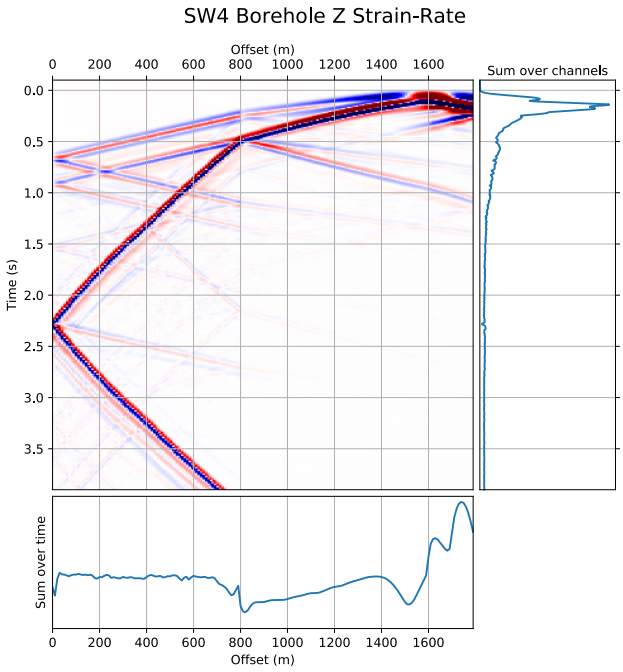

Figure 17 – SW4 strain-rate synthetics for the revised North Sea model recorded along the borehole array. Channel 0 is located at the surface, with the base of the array at 2000 m depth. The source is located at a depth of 1630 m.

7 Conclusions and Recommendations

Through a series of progressively more complex models we have shown that we can achieve reasonably consistent synthetic DAS data using both SW4 and SPECFEM3D. This gives confidence that the wavefields are accurately being modelled, such that either method can be used to create synthetic data for DigiMon. However, through this analysis we identified some differences in the capabilities of each modelling method such that, depending on the use case, one method may offer advantages over the other. These are summarised below:

Array geometry: One of the benefits of DAS systems is that they provide a very dense sampling of the wavefield, with channel spacing on the order of a metre. However, this close spacing presents a challenge for modelling DAS synthetics with SW4, as receivers must be at mesh nodes (e.g. A grid spacing of 8 means that the receivers cannot be closer than 8 meters). In contrast SPECFEM3D allows receivers to be placed at any location within the mesh, allowing for more flexibility in modelled array geometries.

Boundary effects: To suppress boundary effects at the lateral sides of the model geometry each model employed a form of absorbing boundary conditions. The SW4 models used supergrid boundaries and the SPECFEM3D models used Stacey boundary conditions. The SW4 models greatly outperformed SPECFEM in this respect. Clear boundary reflections could be seen in the SPECFEM models, which then interfered with later arrivals. The boundary conditions of SPECFEM models could possibly be improved by using more sophisticated absorbing boundary conditions like perfectly matched layer (PMLs).

Strain output: One of the major benefits of SW4 over SPECFEM is that it supports the direct output of strain seismograms for all 6 independent components of the strain tensor. In contrast, SPECFEM supports only the output of 3 component particle motion seismograms, and the conversion to strain must be done through numerical differentiation in post processing. This is not a significant weakness when simulating simple linear fibres, where only the axial strain needs to be modelled. However, there are scenarios where having the full strain tensor output would be desirable, for example in modelling the response of helically wound cables which are sensitive to strain in multiple directions.

8 References

Castagna, J.P., Batzle, M.L. & Eastwood, R.L. Relationships between compressional-wave and shear-wave velocities in clastic silicate rocks. Geophysics, 50, 571–581, 1985.

Komatitsch, D., and Tromp, J. Introduction to the spectral element method for three-dimensional seismic wave propagation. Geophysical journal international 139, 3 (1999), 806–822.

Mavko, G., Mukerji, T., and Dvorkin, J. The rock physics handbook: Tools for seismic analysis of porous media. Cambridge University Press, 2009.

Peter, D., Komatitsch, D., Luo, Y., Martin, R., Le Goff, N., Casarotti, E., Le Loher, P., Magnoni, F., Liu, Q., Blitz, C., et al. Forward and adjoint simulations of seismic wave propagation on fully unstructured hexahedral meshes. Geophysical Journal International 186, 2 (2011), 721–739.

Petersson, N. A., and Sjögreen, B. High order accurate finite difference modeling of seismo-acoustic wave propagation in a moving atmosphere and a heterogeneous earth model coupled across a realistic topography. Journal of Scientific Computing 74, 1 (2018), 290–323.

Pluymaekers, M. P. D., Doornenbal, J. C., and Middelburg, H. Velmod-3.1. Tech. Rep. R11014, TNO, 2017.

Sjögreen, B., and Petersson, N. A. A fourth order accurate finite difference scheme for the elastic wave equation in second order formulation. Journal of Scientific Computing 52, 1 (2012), 17–48.

Tromp, J., Komattisch, D., and Liu, Q. Spectral-element and adjoint methods in seismology. Communications in Computational Physics 3, 1 (2008), 1–32.